IEEE Photonics Journal
An IEEE Photonics Society Publication

Open Access

# Advanced Electrode Design for Low-Voltage High-Speed Thin-Film Lithium Niobate Modulators

Volume 13, Number 2, April 2021

Xingrui Huang
Yang Liu
Zezheng Li
Huan Guan
Qingquan Wei
Zhiguo Yu
Zhiyong Li

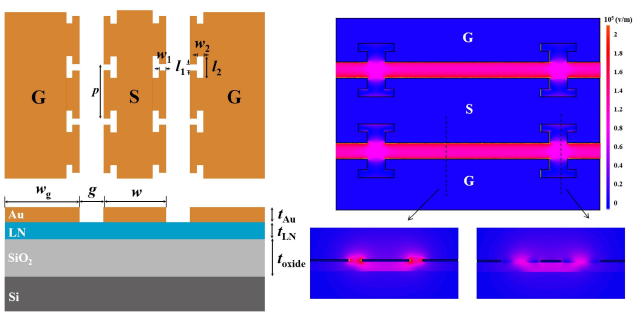


DOI: 10.1109/JPHOT.2021.3066159

IEEE photonics SOCIETY

IEEE

# Advanced Electrode Design for Low-Voltage High-Speed Thin-Film Lithium Niobate Modulators

**Xingrui Huang**,[1,2] **Yang Liu**,[1,2] **Zezheng Li**,[1,2] **Huan Guan**,[1] **Qingquan Wei**,[1] **Zhiguo Yu**,[1] **and Zhiyong Li**[1]

[1]State Key Laboratory on Integrated Optoelectronics, Institute of Semiconductors, Chinese Academy of Sciences, Beijing 100083, China
[2]College of Materials Science and Opto-Electronic Technology, University of Chinese Academy of Sciences, Beijing 100083, China

*DOI:10.1109/JPHOT.2021.3066159*


Manuscript received January 17, 2021; accepted March 10, 2021. Date of publication March 15, 2021; date of current version April 1, 2021. This work was sponsored by the National Key Research and Development Program of China under Grant 2019YFB2203802. Corresponding author: Zhiyong Li (e-mail:lizhy@semi.ac.cn).

**Abstract:** In this paper, we present a novel transmission line architecture in thin-film lithium niobate (TFLN) platforms to improve the velocity match between the microwave and the optical wave. Compared to conventional coplanar waveguide (CPW), the microwave index ($n_m$) of the proposed slotted electrodes can be optimized from 2.1 to 3 while maintaining the high modulation efficiency and 50-Ω impedance match. Equivalent-circuit model analysis and finite-element simulation are performed. The simulated half-wave voltage ($V_\pi$) of 1.2 V and E-O modulation bandwidth greater than 80 GHz is obtained for a 2-cm-long modulator. By utilizing the slotted slow-wave electrode, TFLN Mach-Zehnder modulators with CMOS-compatible operating voltage and 3-dB modulation bandwidth greater than 100 GHz are potentialized.

**Index Terms:** Electro-optical systems, optical interconnects, waveguide devices.

## 1. Introduction

The exponential growth of transmission rate in data centers and telecommunication networks demands electro-optic (E-O) modulators with high E-O bandwidth, low operating voltage and linearity response [1]. To address those demands, optical modulators on various platforms have been widely investigated for the last decades, such as silicon-on-insulator (SOI) [2]–[5], indium phosphate (InP) [6], [7], silicon-organic hybrid (SOH) [8], [9], silicon-germanium [10] and thin-film lithium niobate (TFLN) [11]–[18]. Among these platforms, TFLN photonic platform has drawn significant attention. Lithium niobate (LN) is a material that has a ultra-wide transparency window (350–5000 nm), large second order electro-optic coefficient (30 pm/V) and good temperature stability [19]. TFLN combines the excellent material properties of LN and the thin-film advantages of strong optical confinement, making it possible to fabricate chip-scale LN photonic integrated circuits. Low voltage and ultrahigh bandwidth Mach-Zehnder modulators have been demonstrated in TFLN platforms [11]–[18].

Achieving high-speed TFLN modulators with CMOS-compatible operating voltage is the primary goal in the research field. However, the commonly applied method to lower half-wave voltage is

TABLE 1
Comparison of Reported Mach-Zehnder Modulators on TFLN Platforms

| Platform | Optical group index $n_g$ | Microwave index $n_m$ | Characteristic impedance $Z_c$ ($\Omega$) | $\Delta$n-limited bandwidth $^*f_{3dB}$ (GHz) |
|---|---|---|---|---|
| $SiN_x$-TFLN [21] | 2.16 | 2.09 | 58 | 96 |
| $SiN_x$-TFLN [22] | 2.05 | 2.45 | 50 | 17 |
| SiP-TFLN [11] | 2.21 | 2.13 | 50 | 83 |
| SiP-TFLN [17] | 2.32 | 2.25 | 50 | 96 |
| Etched-LN [23] | 2.24 | 2.26 | 30 | 332 |
| Etched-LN [24] | 2.25 | 2.15 | 50 | 67 |

*The bandwidth is calculated using the equation in [25]: $f_{3\,dB} = \frac{1.39 \cdot c}{\pi \cdot L \cdot \Delta n}$, where $\Delta n = |n_g - n_m|$ and $L = 2$ *cm*.

increasing the phase shifter length, which brings great challenges to the transmission line design. For a high-speed traveling-wave Mach-Zehnder modulator design, there are three major factors need to be fulfilled: the velocity match between the microwave and optical wave, the impedance match of the traveling-wave electrode and low microwave attenuation. However, as shown in Tabel 1, for modulators with 2-cm-long phase shifters, the modulation bandwidth limited by velocity mismatch only in reported platforms is mostly lower than 100 GHz. Combined with other limiting factors such as lossy conductor and impedance mismatch, the experimental results showed limited bandwidth of 26$\sim$40 GHz [16], [20].

The cause of the velocity mismatch in reported modulators can be list as follows:

(i) the use of thick buried oxide layer [16] or low permittivity substrate [23]. employing this kind of substrate will significantly reduce the refractive index of the medium around the electrode, resulting in low microwave index as low as 2.02 [23].

(ii) the use of high refractive index material in hybrid rib-loading platforms, such as amorphous silicon [26] and silicon-rich nitride [27]. The optical group index ($n_g$) of those hybrid waveguides can be as high as 2.8, which makes the velocity match difficult to be achieved. But on the other hand, the modulation efficiency is enhanced due to more electro-optical interaction time, and the high index contrast between rib-loading material and LN can offer a tight optical confinement.

(iii) the trade-off between modulation efficiency and modulation bandwidth in conventional coplanar waveguide (CPW) electrode, which is the main limitation of high-speed modulation performance in reported TFLN modulators. Firstly, the width of the electrode gap is selected as the minimum value with tolerable metal absorption loss, which is typically 5$\sim$8 $\mu$m wide. Secondly, the characteristic impedance should equal the source impedance to reduce reflection. Under these two preconditions above, the microwave index $n_m$ of the traveling-wave electrode is determined, and it can't be modified without affecting the impedance match or the modulation efficiency.

A number of compromise solutions have been implemented to avoid this dilemma [12], [15], [16], [23]. In [23], the velocity match was achieved at the expense of small characteristic impedance ($<$30 $\Omega$), which caused serious reflection and limited the modulation bandwidth. In [12], the buried oxide thickness was increased to lower the microwave refractive index, but, the substrate specifications are limited by the manufacturing process and it will affect other performances of the modulator, such as mode leakage and coupling loss [28]. Thus, the velocity mismatch and impedance mismatch in TFLN modulator design, especially when low refractive index substrate or high refractive index material is used, has yet to be resolved.

To address these limitations, we propose the slotted slow-wave electrode in thin-film lithium niobate (TFLN) platforms. The microwave index ($n_m$) of the slotted electrode can be optimized to achieve velocity match while maintaining high modulation efficiency and impedance match. Equivalent-circuit model analysis and finite-element simulation are performed. A large range of velocity match (2.1 $\sim$3) can be realized with adjustable microwave refractive index. The simulated

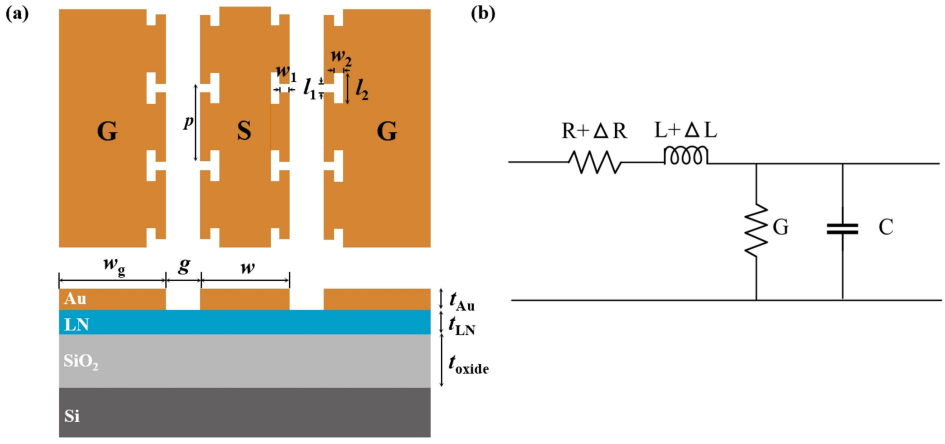


Fig. 1. (a) Top and cross-section view of the slotted slow-wave electrode with design parameters labelled. (b) Transmission line equivalent circuit model of the electrode.

E-O 3-dB $S_{21}$ of 81 GHz is obtained for a 2-cm-long modulator. This approach is capable of low-voltage and high-speed modulation with flexible waveguide design.

## 2. Design of the Slotted Slow-Wave Electrode

### *2.1 Device Concept and Equivalent Circuit Analysis*

Slow-wave electrodes have been widely explored in III-V compound modulators to slow down the microwave signal [29]–[31]. This type of design is usually realized using periodically loaded structures and it is non-uniform along the propagation direction. A capacitively loaded structure, called T-rail electrode, was proposed with the equivalent circuit and analytical loss expressions in [31]. In TFLN platforms, slow-wave electrode has only been used to reduce microwave loss in [32].

Fig. 1(a) shows the top and cross-section view of the proposed slotted slow-wave electrode. The electrodes are deposited on top of x-cut lithium niobate-on-insulator (LNOI) substrate, in which TFLN is bonded on thermal oxidized silica and the substrate is 500- $\mu$m silicon. LNOI substrates with different specifications are commercially available (NANOLN Inc.) and the specifications need to be chosen carefully. In this work, the thickness of thermal oxidized silica ($t_{\text{oxide}} = 4.7$ $\mu$m) is fixed as 4.7 $\mu$m, which is a compromise between optical mode leakage and microwave loss and widely used in modulator design [16], [20]. Besides, the thickness of TFLN ($t_{\text{LN}} = 400$ nm) is chosen as 400 nm to simply the simulation. The propagation direction of the microwave is perpendicular to the Z-axis of lithium niobate to maximize the modulation efficiency. The periodic slots partially cut off the current path and increase the impedance and inductance of the electrode, which will significantly affect the RF parameters. Thus, compared to traditional CPW, The slotted electrode has adjustable RF parameters by controlling the slot parameters while high modulation efficiency and impedance match are ensured. The additional resistance and impedance caused by the slots are mainly determined by the dimensions $l_2$, $w_2$ $l_1$ and $p$. As explained in [33], the period of the slots need to be chosen carefully to make sure the Bragg cut-off frequency is much higher than operating frequency. Here the period $p$ is designed to be 50 $\mu$m, making cut-off frequency approximately over 1000 GHz. In addition, The length $l_1$ of the slots is fixed as 5 $\mu$m in our design to minimize the negative impact on modulation efficiency, which will be fully discussed later in Section 2.2. The transmission line equivalent circuit is shown in Fig. 1(b), $R$, $L$, $G$ and $C$ are the impedance, inductance, conductance and capacitance per unit length of the CPW. $\Delta R$ and $\Delta L$ are the impedance and inductance per unit length as a result of the periodic slots. Combined with the transmission line theory [34], the characteristic impedance $Z_c$ and the microwave index $n_m$ are

given by

$$Z_c = \sqrt{\frac{(R + \Delta R) + j\omega(L + \Delta L)}{G + j\omega C}} \tag{1}$$

$$\gamma = \sqrt{[(R + \Delta R) + j\omega(L + \Delta L)](G + j\omega C)} = \alpha + j\beta \tag{2}$$

$$n_m = \frac{c\beta}{\omega} \tag{3}$$

where $\omega$ is the angular frequency, $c$ is the speed of light in vacuum, $\gamma$, $\alpha$ and $\beta$ are the propagation constant, the attenuation constant and the phase constant, respectively.

At frequency higher than 10 GHz, the capacitance and inductance become the dominant factors in (1) and (2) ($\omega C/G > 1000$ and $\omega L/R > 20$), then we have:

$$C = \frac{n_m}{c \cdot Z_c} \quad \text{and} \quad L + \Delta L = \frac{Z_c \cdot n_m}{c} \tag{4}$$

In (4), one can see that the additional inductance $\Delta L$ caused by the periodic slots will significantly increase the microwave index, and in other words, slow down the microwave signal. The target value of $Z_c$ is usually 50 Ω and $n_m$ should be modified to match the optical group index $n_g$. Thus, the demand value of $C$, $L + \Delta L$ can be calculated by (4). When the width of the electrode gap is determined, the value of $C$ is mainly affected by the width of the signal electrode, which can be accurately calculated by quasi-TEM analysis and conformal transformation [35]. Then, with known $C$ and $L$, one can choose the suitable parameters of the slot to get the required $\Delta L$. However, the electromagnetic field at the slot area is not a quasi-TEM mode and the fringing field is complex around the edge of the slot. Therefore, the analysis formulas of $\Delta R$ and $\Delta L$ are difficult to obtain. In previous studies of capacitively loaded slow wave structure [14], [15], the accurately value of the capacitively load was obtained from the model fitting to experimental results. Here, to get the accurately value of $\Delta R$ and $\Delta L$, numerical finite-element simulations are performed using commercial 3-D electromagnetism simulator.

The signal electrode width $w$ and the slot length $l_2$ have significant influence on microwave parameters, which is the main variable parameters in our simulation, and other parameters are fixed as: $p = 50$ $\mu$m, $t_{Au} = 1$ $\mu$m, $w_1 = 4$ $\mu$m, $w_2 = 3$ $\mu$m, $l_1 = 5$ $\mu$m, $g = 6$ $\mu$m. It should be noted that if a bigger microwave refractive index is required, it might be necessary to choose a smaller period $p$ and a larger slot width $w_2$, and vice versa. In order to confirm whether the equivalent circuit is correct, we analysis simulated S-parameters of the slot electrodes with different lengths of $l_2$ and a fixed signal electrode width ($w = 24$ $\mu$m). Fig. 2 shows the RF parameters $R_{total}$ ($R_{total} = R + \Delta R$), $L_{total}$ ($L_{total} = L + \Delta L$) and $C_{total}$ ($C_{total} = C + \Delta C$) extracted from the simulated S-parameters. Compared to the conventional CPW, the inductance and resistance per unit length of the slow-wave electrode is much higher and increase along with the increasing $l_2$ while the capacitance per unit length is barely the same. Therefore, the simulation results are consistent with the equivalent circuit analysis and prove the validity of the circuit model.

Choosing the appropriate $w$ and $l_2$ is the key to get the desired $n_m$ and 50-Ω impedance match. Fig. 3(b) presents contour maps of $n_m$ and $Z_c$ as a function of the signal electrode width $w$ and the slot length $l_2$. Under the selected substrate specifications and electrode parameters, the highest $n_m$ in our simulation is 2.99 with $l_2 = 45$ $\mu$m and $w = 20$ $\mu$m, and the lowest $n_m$ is 2.26 with $l_2 = 5$ $\mu$m and $w = 20$ $\mu$m. The microwave index of traditional CPW electrodes is 2.08 under the condition of impedance matching and 6- $\mu$m electrode gap, so the range from 2.08 to 2.26 can be obtained by choosing smaller slot dimensions or longer period. In the range of $n_m > 3$, a wider signal electrode is needed to get the required value of $C$ according to (4), which is not included in our simulation. In aggregate, this slotted slow-wave electrode can achieve a range of $N_m$ from 2.1 to 3 with impedance match and 6- $\mu$m electrode gap.

Besides, it is worth noting that the inductance $\Delta L$ induced by the slots drop rapidly with increasing signal electrode width while the capacitance $C$ rises much slower. Hence, the microwave index $n_m$

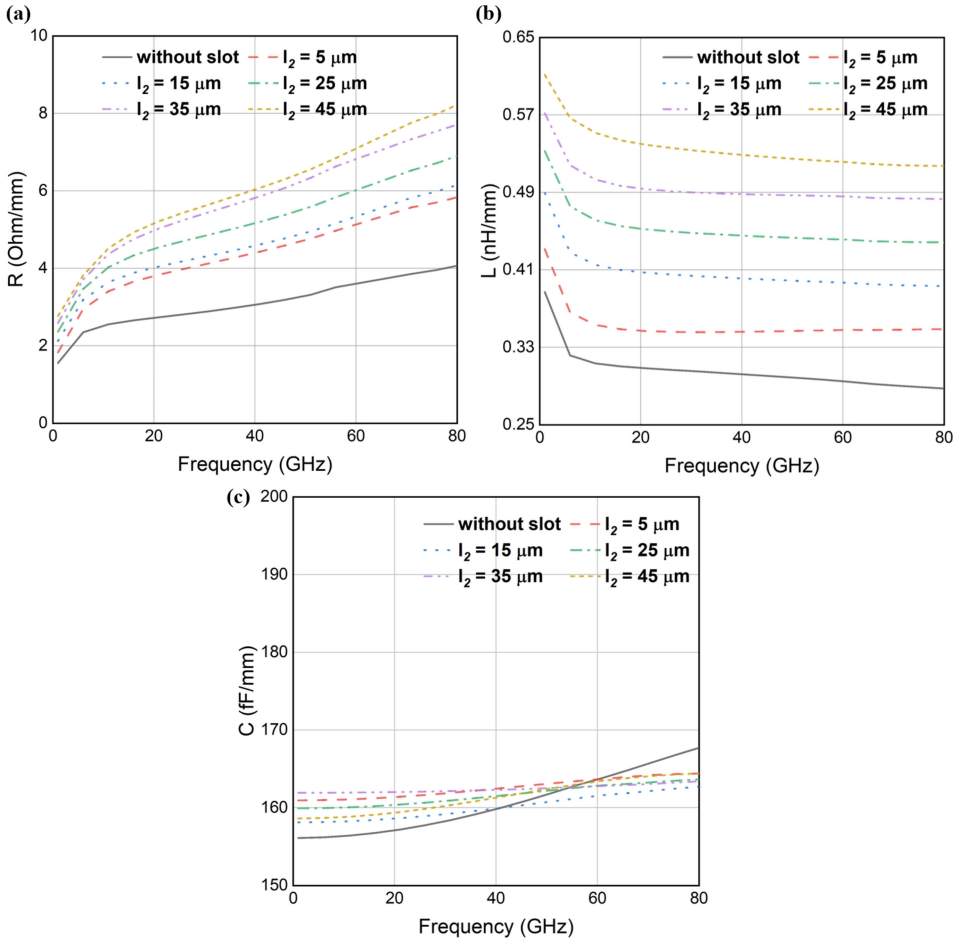


Fig. 2. Simulated resistance $R_{\text{total}}$ (a), inductance $L_{\text{total}}$ (b) and capacitance $C_{\text{total}}$ (c) for different slot dimensions as a function of frequency.

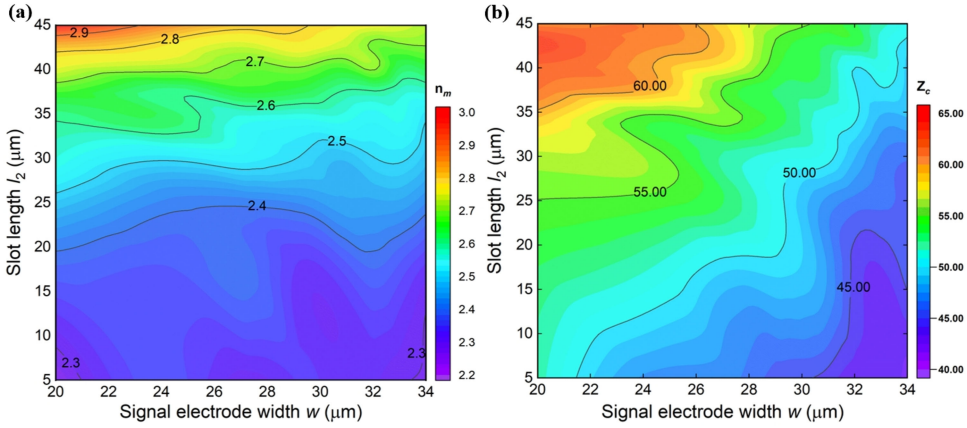


Fig. 3. Contour maps of $n_m$ (a) and $Z_c$ (b) as a function of the signal electrode width $w$ and the slot length $l_2$. The width of the electrode gap is fixed as 6 $\mu$m and the parameters are simulated at 20 GHz.

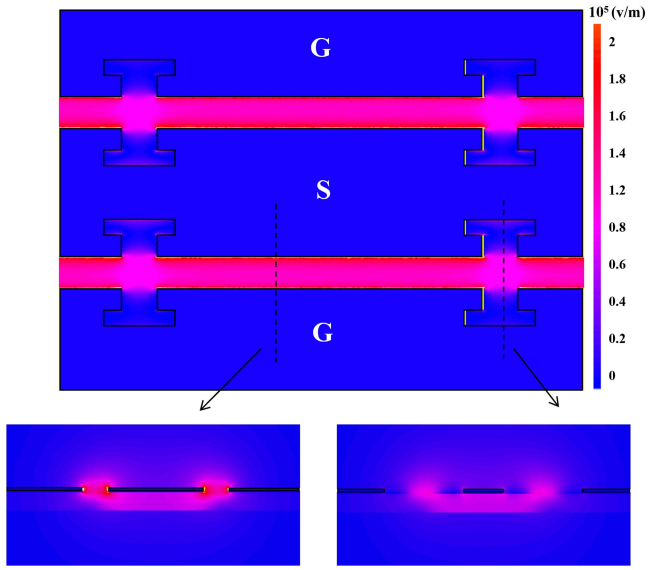


Fig. 4. Simulated electric field intensity along Z-direction ($E_z$) of the slotted electrodes and mode distributions in the cross-section view.

does not rise but decreases as the signal width increases, which is the opposite of the traditional CPW.

### 2.2 Influence on Modulation Efficiency

Modulation efficiency is also an important part of the modulator performance, improving the modulation efficiency can help on reducing the phase shifter length, which is negatively correlated with the modulation bandwidth. The modulation efficiency figure-of-merit ($V_\pi \cdot L$) can be written as:

$$V_\pi \cdot L = \frac{n_{eff}\lambda_o}{2{n_e}^4 r_{33}\Gamma} \tag{5}$$

$$\Gamma = \frac{\iint |\mathbf{E_o}|^2 E_z ds}{\iint |\mathbf{E_o}|^2 ds} \tag{6}$$

where $n_{eff}$ is the effective index of optical mode, $\lambda_o$ is the operation wavelength, $n_e$ is the extraordinary refraction index of LN, $r_{33}$ is the electro-optical coefficient (31 pm/V), $\Gamma$ is the overlap factor between optical mode ($|\mathbf{E}_o|$) and electric field normalized to the applied voltage along the Z-axis ($E_z$).

$V_\pi \cdot L$ is mostly determined by $E_z$ in 5, the simulated electric field intensity along Z-direction ($E_z$) of the slotted electrodes is shown in Fig. 4. The supply voltage is 1 V in this simulation. It can be seen that the electric field is weakly distributed near the slots and not constant along the propagation direction. For the non-slotted area, the $E_z$ in the middle of the electrode gap is found to be $1.35 \times 10^5$ V/m, which is similar to that of the conventional CPW with same width of electrode gap. For the slotted area, the $E_z$ in the middle of the electrode gap is around $1 \sim 1.1 \times 10^5$ V/m, which is approximately 20% lower than that of the non-slotted area.This lower electric field intensity will affect the modulation efficiency, but by using this T-shape slot, the degree of slow-wave effect can be adjusted by other dimensions of the slot while keeping the breach width $l_1$ as small as possible. Thus with proper design, slotted electrodes will only cause a very slight drop in modulation efficiency.

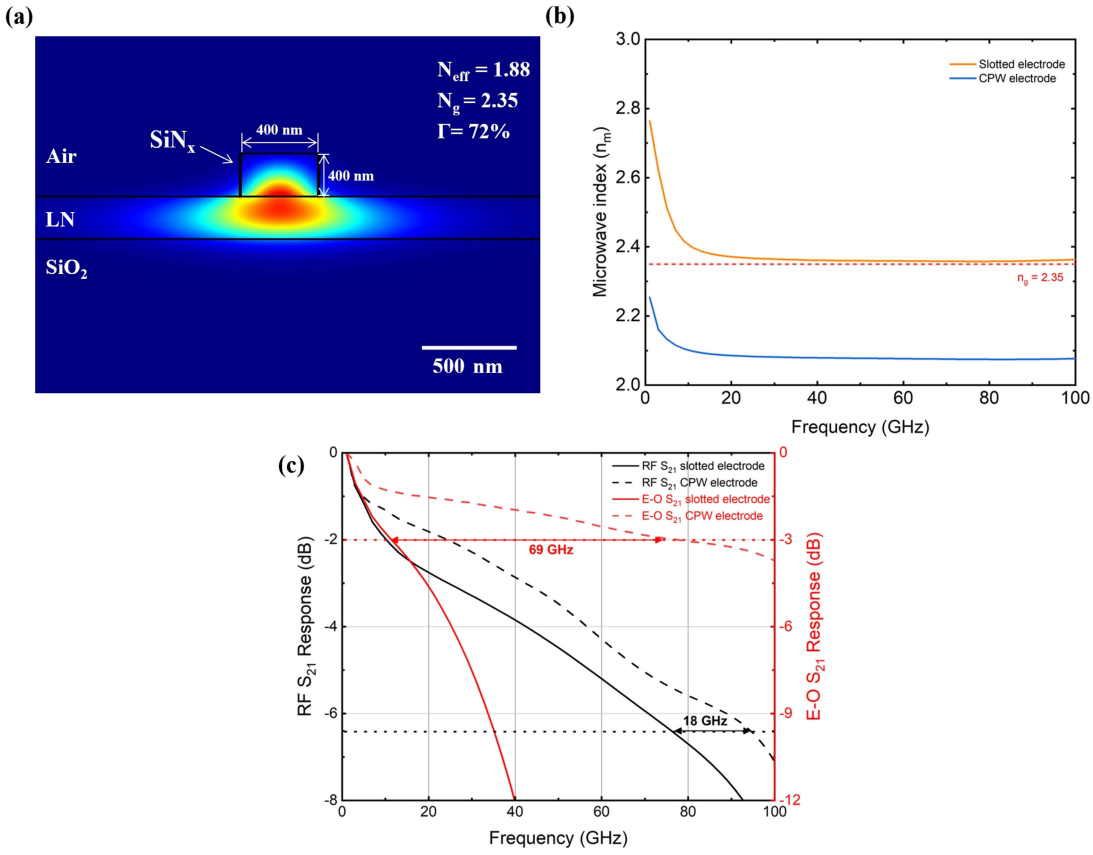


Fig. 5. (a) Simulated TE optical mode profile with 400-nm-thick LN and 400-nm-tall, 400-nm-wide silicon-rich nitride ridge waveguide. (b) Simulated microwave index of the slotted slow-wave electrode and the conventional CPW electrode. (c) Simulated RF S21 (left Y axis) and E-O S21 (right Y axis) of 2-cm-long modulators with the slotted slow-wave electrode and the conventional CPW electrode.

### *2.3 Modulation Bandwidth*

To prove the advantages of this slotted slow-wave electrode in high-speed and low-voltage modulation, here we adopt the waveguide design in our previous work [27]. The rib-loaded waveguide is formed consisting of 400-nm silicon-rich nitride ridge layer ($n = 2.501$ at 1550 nm) and 400-nm LN slab layer. This hybrid rib-loaded waveguide can achieve both low bending radius (50 $\mu$m) and high modulation efficiency.

The simulated optical TE mode profile at 1550 nm wavelength is shown in Fig. 5(a), the optical mode confined in LN slab is greater than 72%, and the waveguide group index $n_o$ is 2.35. On the condition of 6- $\mu$m electrode gap and 50-$\Omega$ impedance match ($g = 6$ $\mu$m and $w = 16$ $\mu$m), $n_m$ of the conventional CPW electrode is 2.08, which is 0.27 different from $n_g$. This condition requires the use of slow-wave electrodes with optimized dimensions. Based on the aforementioned discussion, the slot dimensions are chosen as: $p = 50$ $\mu$m, $t_{Au} = 1$ $\mu$m, $w_1 = 4$ $\mu$m, $w_2 = 3$ $\mu$m, $l_1 = 5$ $\mu$m, $w = 24$ $\mu$m, $l_2 = 10$ $\mu$m. As is shown ub Fig. 5(b), the simulated $n_m$ of the optimized slotted electrode is around 2.36 from 10 to 100 GHz, which indicates that the velocity mismatch is almost eliminated ($\Delta n < 0.01$).

Fig. 5(c) shows the simulated RF S21 and E-O S21 of 2-cm-long modulators with the slotted slow-wave electrode and the conventional CPW electrode. The $-6.4$ dB RF $S_{21}$ of the slotted electrode is 95 GHz, which is 18 GHz higher than that of the traditional CPW. The E-O response is

calculated from the equation given in [25]:

$$r(\omega_m) = \left| \frac{1 - \rho 1 \cdot \rho 2}{1 + \rho 2} \cdot \frac{V_+ + \rho 2 \cdot V_-}{e^{\gamma \cdot l} - \rho 1 \cdot \rho 2 \cdot e^{-\gamma \cdot l}} \right| \tag{7}$$

where r($\omega_m$) is the modulation response, $\rho_1 = (Z_c - Z_s)/(Z_c + Z_s)$ and $\rho_2 = (Z_t - Z_s)/(Z_t + Z_s)$ are the input and output reflection coefficient, $Z_s$ and $Z_t$ are the source impedance and terminating impedance. $V_+$ and $V_-$ are the single pass average voltage experienced by a photon due to co-propagation and counter-propagation between microwave and optical wave, where $V_\pm = e^{\pm j \cdot \phi_\pm} \cdot (sin\phi_\pm/\phi_\pm)$ and $\phi_\pm = l/2 \cdot (-j \cdot \gamma \mp \beta_o)$, and $\beta_o$ is the complex phase of optical wave.

The calculated 3-dB E-O bandwidth of conventional CPW is 12 GHz, which is mainly limited by the velocity mismatch ($\Delta n = 0.27$). By contrast, the 3-dB E-O bandwidth of the slotted electrode is 81 GHz and it is close to the RF $-6.4$ dB bandwidth. One must note that the microwave loss is taken into consideration in (7), the E-O bandwidth can be further improved with thicker electrode or optimized substrate specification. This simulated result indicates that, for a low-voltage TFLN modulator design, the slotted slow-wave electrodes have advantages of higher E-O bandwidth compared to conventional CPW electrodes. The calculated $V_\pi \cdot L$ of the slotted electrode and the conventional CPW are almost at the same. Which are 2.32 V $\cdot$ cm and 2.28 V $\cdot$ cm, respectively.

As presented above, the key advantage of the slotted slow-wave electrode is that velocity mismatch can be almost eliminated, which is the main bandwidth limiting factor in the low-voltage modulator design. In addition, the fabrication of this slotted slow-wave electrode does not require any complex manufacturing process and it can be done with one-step lithography and standard lift-off process.

## 3. Conclusion

In summary, the slotted slow-wave electrode in thin-film lithium niobate (TFLN) platforms are proposed. Compared to conventional CPW electrodes, the microwave index of slotted electrodes can be adjusted among a large range (2.3$\sim$3) while maintaining high modulation efficiency and impedance match. Equivalent-circuit model is proposed and finite-element simulation of the slotted electrode is performed. By utilizing this approach, the limitation of E-O bandwidth due to velocity mismatch can be eliminated and The E-O 3-dB bandwidth of a 2-cm-long modulator is expected to reach 81 GHz, which is 69 GHz larger than that of the modulator with CPW electrodes. This approach has great potential to achieve sub-1 V operating voltage and high-speed modulation up to 100 GHz.

## Acknowledgment

The authors thank and L. Liu for helpful discussions.

## References

[1] G. T. Reed, G. Mashanovich, F. Y. Gardes, and D. J. Thomson, "Silicon optical modulators," *Nature Photon.*, vol. 4, no. 8, pp. 518–526, 2010.
[2] M. Li, L. Wang, X. Li, X. Xiao, and S. Yu, "Silicon intensity Mach-Zehnder modulator for single lane 100 Gb/s applications," *Photon. Res.*, vol. 6, no. 2, pp. 109–116, 2018.
[3] J. Witzens, "High-speed silicon photonics modulators," *Proc. IEEE*, vol. 106, no. 12, pp. 2158–2182, Dec. 2018.
[4] H. Xu *et al.*, "High speed silicon Mach-Zehnder modulator based on interleaved pn junctions," *Opt. Exp.*, vol. 20, no. 14, pp. 15093–15099, 2012.
[5] H. Xu *et al.*, "High-speed silicon modulator with band equalization," *Opt. Lett*, vol. 39, no. 16, pp. 4839–42, 2014.
[6] S. Lange *et al.*, "100 gbd intensity modulation and direct detection with an inp-based monolithic dfb laser Mach-Zehnder modulator," *J. Lightw. Technol.*, vol. 36, no. 1, pp. 97–102, 2018.
[7] Y. Ogiso *et al.*, "80-GHz bandwidth and 1.5-v vpi inp-based iq modulator," *J. Lightw. Technol.*, vol. 38, no. 2, pp. 249–255, 2020.
[8] L. Alloatti *et al.*, "100 GHz silicon-organic hybrid modulator," *Light: Sci. Appl.*, vol. 3, no. 5, pp. e173–e173, 2014.
[9] S. Wolf *et al.*, "Coherent modulation up to 100 GBd 16QAM using silicon-organic hybrid (SOH) devices," *Opt. Exp.*, vol. 26, no. 1, pp. 220–232, 2018.

[10] L. Mastronardi *et al.*, "High-speed Si/GeSi hetero-structure electro absorption modulator," *Opt. Exp.*, vol. 26, no. 6, pp. 6663–6673, 2018.
[11] M. He *et al.*, "High-performance hybrid silicon and lithium niobate Mach-Zehnder modulators for 100 gbits-1 and beyond," *Nature Photon.*, vol. 13, no. 5, pp. 359–364, 2019.
[12] A. Honardoost, F. A. Juneghani, R. Safian, and S. Fathpour, "Towards subterahertz bandwidth ultracompact lithium niobate electrooptic modulators," *Opt. Exp.*, vol. 27, no. 5, pp. 6495–6501, 2019.
[13] S. Jin, L. Xu, H. Zhang, and Y. Li, "$LiNbO_3$ thin-film modulators using silicon nitride surface ridge waveguides," *IEEE Photon. Technol. Lett.*, vol. 28, no. 7, pp. 736–739, Apr. 2016.
[14] A. Rao *et al.*, "High-performance and linear thin-film lithium niobate Mach-Zehnder modulators on silicon up to 50 GHz," *Opt. Lett.*, vol. 41, no. 24, pp. 5700–5703, 2016.
[15] C. Wang, M. Zhang, B. Stern, M. Lipson, and M. Loncar, "Nanophotonic lithium niobate electro-optic modulators," *Opt. Exp.*, vol. 26, no. 2, pp. 1547–1555, 2018.
[16] C. Wang *et al.*, "Integrated lithium niobate electro-optic modulators operating at cmos-compatible voltages," *Nature*, vol. 562, no. 7725, pp. 101–104, 2018.
[17] P. O. Weigel *et al.*, "Bonded thin film lithium niobate modulator on a silicon photonics platform exceeding 100 GHz 3-db electrical modulation bandwidth," *Opt. Exp.*, vol. 26, no. 18, pp. 23 728–23 739, 2018.
[18] M. Xu *et al.*, "Michelson interferometer modulator based on hybrid silicon and lithium niobate platform," *APL Photon.*, vol. 4, no. 10, 2019, Art. no. 100802.
[19] L. Arizmendi, "Photonic applications of lithium niobate crystals," *Physica Status Solidi (a)*, vol. 201, no. 2, pp. 253–283, 2004.
[20] A. N. R. Ahmed, S. Shi, A. Mercante, S. Nelan, P. Yao, and D. W. Prather, "High-efficiency lithium niobate modulator for k band operation," *APL Photon.*, vol. 5, no. 9, 2020, Art. no. 091302.
[21] A. N. R. Ahmed, S. Shi, A. J. Mercante, and D. W. Prather, "High-performance racetrack resonator in silicon nitride - thin film lithium niobate hybrid platform," *Opt. Exp.*, vol. 27, no. 21, pp. 30 741–30 751, 2019.
[22] N. Boynton *et al.*, "A heterogeneously integrated silicon photonic/lithium niobate travelling wave electro-optic modulator," *Opt. Exp.*, vol. 28, no. 2, pp. 1868–1884, 2020.
[23] A. J. Mercante, S. Shi, P. Yao, L. Xie, R. M. Weikle, and D. W. Prather, "Thin film lithium niobate electro-optic modulator with terahertz operating bandwidth," *Opt. Exp.*, vol. 26, no. 11, pp. 14810–14816, 2018.
[24] S. Sun *et al.*, "High-speed modulator with integrated termination resistor based on hybrid silicon and lithium niobate platform," *J. Lightw. Technol.*, vol. 39, no. 4, pp. 1108–1115, 2021.
[25] S. H. Lin and S. Y. Wang, "High-throughput gaas pin electrooptic modulator with a 3-db bandwidth of 9.6 GHz at 1.3 $\mu$-m," *Appl. Opt.*, vol. 26, no. 9, pp. 1696–1700, 1987.
[26] L. Cao, A. Aboketaf, Z. Wang, and S. Preble, "Hybrid amorphous silicon (a-Si: H)$LiNbO_3$ electro-optic modulator," *Opt. Commun.*, vol. 330, pp. 40–44, 2014.
[27] Y. Liu, X. Huang, Z. Li, H. Guan, Q. Wei, Z. Fan, W. Han, and Z. Li, "Efficient grating couplers on a thin film lithium niobate-silicon rich nitride hybrid platform," *Opt. Lett.*, vol. 45, no. 24, pp. 6847–6850, 2020.
[28] Z. Ruan *et al.*, "Metal based grating coupler on a thin-film lithium niobate waveguide," *Opt. Exp.*, vol. 28, no. 24, pp. 35615–35621, 2020.
[29] A. Gorur, C. Karpuz, and M. Alkan, "Characteristics of periodically loaded CPW structures," *IEEE Microw. Guided Wave Lett.*, vol. 8, no. 8, pp. 278–280, Aug. 1998.
[30] S. JaeHyuk, C. Ozturk, S. R. Sakamoto, Y. J. Chiu, and N. Dagli, "Novel T-rail electrodes for substrate removed low-voltage high-speed GaAs/AlGaAs electrooptic modulators," *IEEE Trans. Microw. Theory Techn.*, vol. 53, no. 2, pp. 636–643, Feb. 2005.
[31] S. JaeHyuk, S. R. Sakamoto, and N. Dagli, "Conductor loss of capacitively loaded slow wave electrodes for high-speed photonic devices," *J. Lightw. Technol.*, vol. 29, no. 1, pp. 48–52, 2011.
[32] P. Kharel, C. Reimer, K. Luke, L. He, and M. Zhang, "Breaking voltage-bandwidth limits in integrated lithium niobate modulators using micro-structured electrodes," *Optica*, vol. 8, no. 3, pp. 357–363, 2021.
[33] D. A. Motta *et al.*, Design of a 40 GHz Bandwidth Slow-Wave Silicon Modulator, *Ser. 2017 Sbmo/Ieee Mtt-S Int. Microw. Optoelectron. Conf.* New York, NY, USA: IEEE, 2017.
[34] R. E. Collin, *Foundations for Microwave Engineering*. New York, NY, USA: McGraw-Hill, 1966.
[35] E. Carlsson and S. Gevorgian, "Conformal mapping of the field and charge distributions in multilayered substrate CPWs," *IEEE Trans. Microw. Theory Techn.*, vol. 47, no. 8, pp. 1544–1552, Aug. 1999.